Tracking the hazy boundary between resonant and normal Auger decay near the K-edges of aqueous K$^+$ and Cl$^-$

Tsveta Miteva,[*,†] Nikolai V. Kryzhevoi,[‡] Nicolas Sisourat,[†] Christophe Nicolas,[¶] Wandared Pokapanich,[§] Thanit Saisopa,[‖] Prayoon Songsiriritthigul,[‖] Yuttakarn Rattanachai,[⊥] Andreas Dreuw,[#] Jan Wenzel,[#] Jérôme Palaudoux,[†] Gunnar Öhrwall,[@] Ralph Püttner,[△] Lorenz S. Cederbaum,[‡] Jean-Pascal Rueff,[†,¶] and Denis Céolin[*,¶]

†Sorbonne Université, CNRS, Laboratoire de Chimie Physique Matière et Rayonnement, UMR 7614, F-75005 Paris, France

‡Theoretische Chemie, Physikalisch-Chemisches Institut, Universität Heidelberg, Im Neuenheimer Feld 229, D-69120 Heidelberg, Germany

¶Synchrotron SOLEIL, l'Orme des Merisiers, Saint-Aubin, F-91192 Gif-sur-Yvette Cedex, France

§Faculty of Science, Nakhon Phanom University, Nakhon Phanom 48000, Thailand

‖School of Physics, Suranaree University of Technology, Nakhon Ratchasima 30000, Thailand

⊥Department of Applied Physics, Faculty of Sciences and Liberal Arts, Rajamangala University of Technology Isan, Nakhon Ratchasima 30000, Thailand

#Interdisciplinary Center for Scientific Computing, Ruprecht-Karls University, Im Neuenheimer Feld 205A, D-69120 Heidelberg, Germany

@MAX IV Laboratory, Lund University, P.O. Box 118, SE-22100 Lund, Sweden

△Fachbereich Physik, Freie Universität Berlin, Arnimallee 14, D-14195, Berlin, Germany

E-mail: tsveta.miteva@upmc.fr; denis.ceolin@synchrotron-soleil.fr

Abstract

    X-ray absorption and Auger electron spectroscopies are powerful tools to probe the electronic structure and immediate surroundings of ions in solution. In this work we use a combination of these methods to study the electronic structure and decay in aqueous KCl at the K-edges of K^+ and Cl^-. Although the two ions are isoelectronic, their Auger electron spectra as a function of the photon energy exhibit notably different features. To explain these differences, we carried out *ab initio* calculations of both the core excited states and the final Auger states of bare K^+, Cl^- and their microsolvated clusters. Our calculations show that the energetic order of the 3d and 4p orbitals is inverted in K^+ with respect to Cl^-. The reverse orbital order in the two ions is reflected in both the ordering of the core excited states and in the final states populated in the resonant Auger decay. The energetic proximity of the 3d and 4p virtual orbitals in the bare K^+ ion leads to their mixing in the presence of the solvent, and to the population of the dipole forbidden $1s^{-1}3d$ state upon K-shell excitation in aqueous solution. The resonant Auger decay of this state results in a separate feature in the Auger electron spectrum of K^+ which is absent in the spectrum of Cl^-. The results of this work represent a pioneering study of the decay processes initiated by photoabsorption in the tender x-ray regime close to threshold in liquids and are thus of importance in unveiling the mechanisms of radiation damage in biologically relevant systems.

Introduction

X-ray absorption and Auger electron spectroscopy are powerful tools to study the electronic structure and the nearest environment of atoms and molecules in gas, liquid and solid phase. Understanding how atoms or molecules respond to irradiation with x-rays gives insight into the structure of solutions (see Ref.[1] and references therein), and the mechanism of radiation damage[2–4]. Upon absorption of an x-ray photon, either core excited or core ionized states of a specific atom are populated depending on the photon energy. The relaxation of these highly energetic states involves an ultrafast cascade of intraatomic processes, such as radiative and

Auger decays. Furthermore, if the initially excited or ionized species is embedded in an environment, interatomic processes such as charge and energy transfer[4–8] are possible.

The course of a decay cascade depends on the character of the initially populated states. This has been well understood in atoms and molecules in gas phase[9–16]. In the case of a core ionized state, the Auger decay process, designated as normal Auger decay (see Fig. 1), leads to the population of doubly ionized final states localized on the initially ionized unit[9–12]. The normal Auger decay process in clusters proceeds similarly to that in atoms or molecules. However, in the case of a core excited state, the resonant Auger process competes with the process of delocalization of the excited electron in clusters. If the initially core excited electron delocalizes within the lifetime of the core hole, then normal instead of resonant Auger decay is observed[17].

In a solution, the electronic decay processes initiated by x-ray photoabsorption are different compared to those in rare gas clusters due to the shorter distances and stronger interatomic interactions. In particular, the solvent molecules have two effects – first, they strongly affect the excited[18] or ionized states of the ion and second, they can participate in the decay processes, leading to the population of charge-separated final states, and ionization of the surrounding environment[4–8]. Moreover, the process of delocalization of the initially excited electron also occurs in aqueous solutions[19,20]. In the case of pure water, the delocalization of the O1s excited electron takes place on a femtosecond to sub-femtosecond time scale depending on the photon energy, thus being commensurate with the lifetime of the O1s core hole which is $\sim$3.6 fs[19]. The O K-edge is located in the soft x-ray range of photon energies, $\sim$533 eV in water vapor[21]. Going higher in photon energy, in the tender and hard x-ray regimes, the lifetimes of the core ionized or core excited states become even shorter, on the order of 1 fs. And thus, it is even more imperative to reveal whether the delocalization of the core excited electron occurs within the lifetime of the core hole.

The aim of this work is to elucidate the nature of the states populated upon x-ray irradiation of solvated ions in the tender x-ray regime, and furthermore, to understand

whether the process of delocalization influences the resonant Auger decay. To this end, we used Auger electron spectroscopy together with x-ray absorption spectroscopy in the tender x-ray regime to study aqueous potassium chloride at the K-edges of both K^+ and Cl^-. In particular, we demonstrate experimentally that at photon energies below the K-edges of the two ions, localized core excited states are populated. These states undergo resonant Auger decay within less than 1 fs. In both ions, there is a competition between resonant Auger decay and delocalization of the excited electron. Using the core-hole clock method we show that in K^+ delocalization at the pre-edge is weak, whereas in the case of Cl^-, due to the energetic proximity of the core excited state to the ionization threshold, the rate of delocalization is of the same order as that of the resonant Auger process. Moreover, we observe that although the K^+ and Cl^- ions are isoelectronic, they have different fingerprints in the resonant Auger spectra. With the aid of high-level *ab initio* calculations of the initial and final states of the resonant Auger process of both the bare ions and their microsolvated clusters, we demonstrate that these differences result from different electronic structures of the two ions, thus confirming that the combination of XAS and AES techniques is a sensitive probe of the electronic structure of solutions.

Methods

Experimental

For the present experiment we used the newly operational microjet setup that was specifically designed for the HAXPES station of the GALAXIES beamline[22,23]. A differentially-pumped tube in which the microjet head is inserted, is mounted on a 3-axes motorized manipulator in front of the spectrometer lens. Two holes of 2 mm diameter allow the photons to go in and out. At the end of the tube and in front of the lens, a 500 μm diameter hole skimmer allows the electrons created at the interaction point to go in the direction of the spectrometer. The microjet head is mostly composed of a 30 μm diameter vertical glass capillary facing a
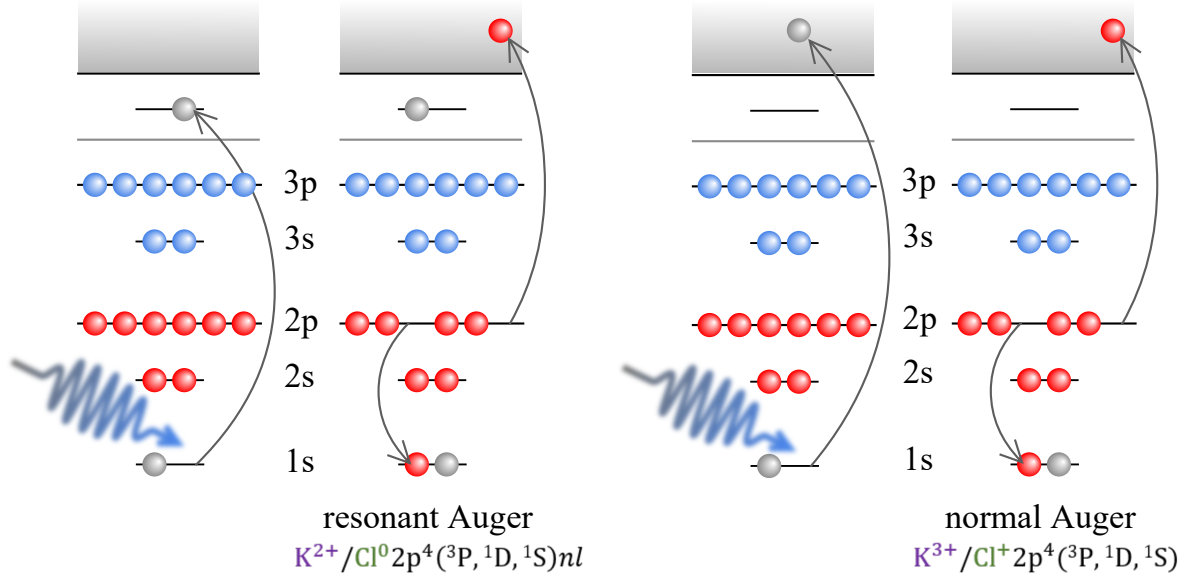
Figure 1: Schematic representation of the resonant (left) and normal (right) Auger processes of the isoelectronic K^+ and Cl^- ions. The charges of the final Auger states in the two ions are also shown.

temperature-controlled catcher in CuBe having a $300\,\mu$m hole, and a camera. Piezo motors allow their precise alignment relative to each other and to the photon beam. The catcher is placed at a distance of about $5\,$mm from the capillary and is permanently pumped in order to extract the liquid. For the present experiment, a 0.5M KCl aqueous solution is injected in the capillary by a high performance liquid chromatography (HPLC) pump with a constant flux of $1.6\,$ml/min. The alignment of the setup is performed on the KCl aqueous solution by measuring the water O1s XPS peak intensity and by optimizing the liquid vs gas phase ratio. The pressure in the main chamber is kept below the $10^{-5}\,$mbar range whereas it is kept at about $10^{-4}\,$mbar in the differentially-pumped tube when the HPLC pump is ON. Our equipment is an updated version of the equipment used in Ref.[24] The aqueous potassium chloride solution was prepared by mixing $>99\%$ KCl salt with deionized water. Filtering and degazing procedures were systematically performed before injecting the solution. The spectrometer resolution of about $0.6\,$eV was achieved with the $500\,$eV pass energy and $0.5\,$mm slits. The photon energy resolution achieved at $2.8\,$keV and $3.6\,$keV was about $0.3\,$eV and $0.4\,$eV, respectively. The experimental 2D maps representing the evolution of the KLL Auger

spectra in the vicinity of the Cl$^-$and K$^+$ K-edges, as a function of the photon energy, are shown in Figs. 2 and 3, respectively. The aqueous K$^+$ and Cl$^-$ 1s ionization potentials were measured at hν=5keV and calibrated on the liquid contribution of the O1s XPS spectrum.[25] The maps were also calibrated using the O1s photoelectron line of liquid water but at photon energies close to the potassium and chloride 1s ionization thresholds.

Ab initio calculations

The theoretical X-ray absorption spectra were computed for the hexa-coordinated clusters of both ions, K$^+$(H$_2$O)$_6$ and Cl$^-$(H$_2$O)$_6$, which can be considered as representatives of the complete first solvation shell of the two ions[26–28]. The two structures shown in Fig. 4 were optimized at the DFT level of theory using the B3LYP functional and the 6-311++G(2d,2p) basis set[29,30]. The geometry optimization was performed with the Gaussian 09 package[31]. In order to obtain realistic structures corresponding to the bulk solution, we carried out constrained geometry optimization by choosing the equilibrium gas-phase geometries[32,33] belonging to the D$_3$ point group and then increasing the angle θ between the K-O/Cl-O bond and the C_3 axis to 55° in the case of K$^+$ and 50° in the case of Cl$^-$. This angle was chosen such that the O-K-O and O-Cl-O angles are around the maxima of the angular distributions obtained from quantum mechanics / molecular mechanics dynamical simulations in Ref.[28]. Moreover, we fixed the K-O and Cl-O distances to 2.840 Å and 3.140 Å, respectively, such that they correspond to the distances from other theoretical and experimental works[26–28,34,35].

The energies and transition moments of the core excited states of the bare ions and micro-solvated clusters were computed with the algebraic diagrammatic construction method for the polarization propagator[36] within the core-valence separation approximation[37–39] (CVS-ADC(2)x) as implemented in the Q-Chem package[40–43]. In the case of Cl$^-$ the 6-311++G(3df,3pd) basis set[29,44] (excluding f functions) was used for all atoms, whereas in the case of K$^+$ we used the 6-311+G(2d,p) basis set[29,30] on all atoms, and two additional sets of s, p and d diffuse functions were added on K. The use of a smaller basis set in the case of K is due to

the higher number of atomic orbitals compared to the case of Cl, and therefore, prohibitively high cost of the CVS-ADC(2)x computation. In our calculations the core space comprises the 1s orbital of K^+ or Cl^-, whereas the remaining occupied orbitals are included in the valence space. For the calculations of the XAS spectra we used the C_2 point group in the case of $K^+(H_2O)_6$ and $Cl^-(H_2O)_6$. To account for the lifetime broadening due to the Auger decay of the core excited states, we convolved the theoretical spectra with a Lorentzian function of FWHM 0.74 eV and 0.62 eV in the case of K^+ and Cl^-, respectively[45]. Additionally, we convolved the theoretical spectra with a Voigt profile to also account for the experimental resolution (see Fig. 4). We analyzed the core excited states by expanding the natural orbitals occupied by the excited electron (singly occupied natural orbitals, SONOs) ψ_i of the microsolvated clusters in the basis of SONOs of the bare K^+ or Cl^- ion χ_{nl}

$$\psi_i = \sum_{nl} a_{nl}^i \chi_{nl} \tag{1}$$

where n and l stand for the principal and orbital quantum numbers as described in Ref.[18]. The expansion coefficients a_{nl}^i show the degree of delocalization of the excited electron and the mixing of the core excited states in the ligand field created by the surrounding water molecules (see Fig. 4).

The final states following KLL resonant Auger decay of $K^+(H_2O)_6$ and $Cl^-(H_2O)_6$ were computed at the Configuration Interaction Singles (CIS) level using the Graphical Unitary Group Approach (GUGA) as implemented in the GAMESS-US package[46–48]. In order to account for the relaxation effects upon core ionization, we used a restricted open-shell Hartree-Fock reference wave function with a hole in the 2s orbital of both K^+ and Cl^-. We used the 6-311++G(2d,2p) basis set[29,30,44] on all atoms. Additionally, the basis set was augmented with two sets of s, p, d diffuse functions in the case of K^+, and three sets of s, p, d diffuse functions in the case of Cl^-. The larger basis set employed in the case of Cl was necessary in order to ensure the convergence of the excited states. The active space comprises the 2s

and 2p orbitals of K/Cl with occupancy fixed to 6 and all virtual orbitals with occupancy fixed to 1. The remaining doubly occupied orbitals were frozen in the calculation.[49]
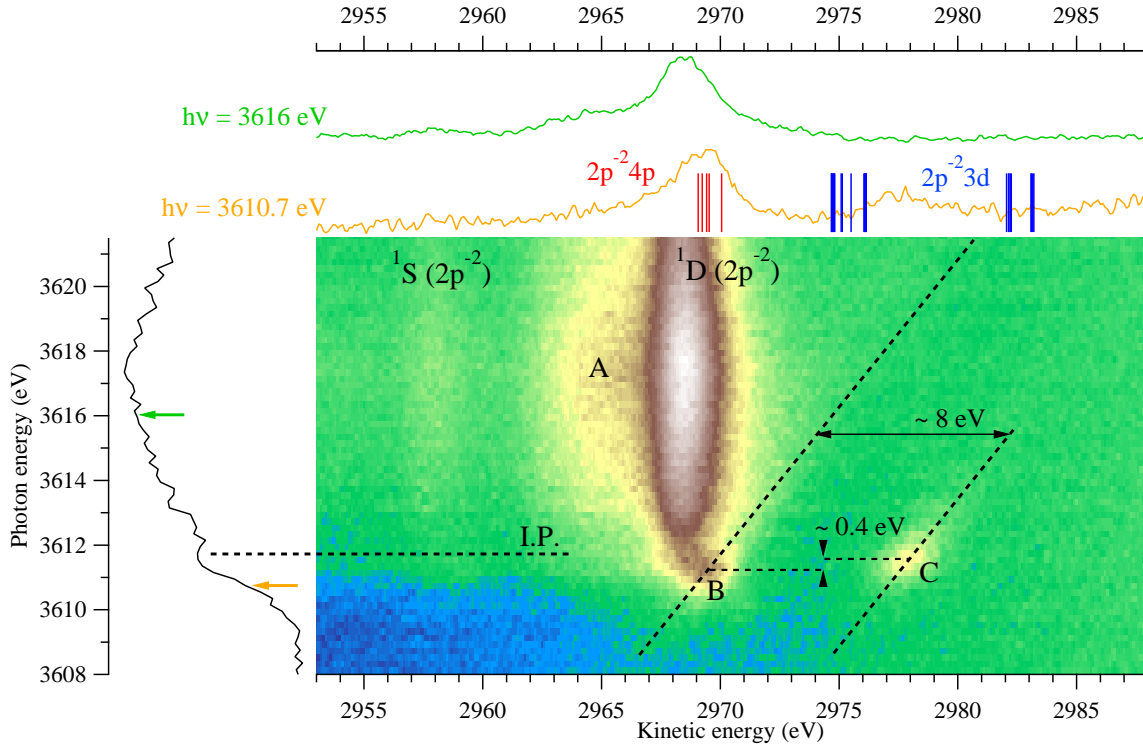
Results and discussion

Figure 2: 2D map showing the kinetic energy of the electrons emitted in $KL_{2,3}L_{2,3}$ Auger decay vs the photon energy in the vicinity of the K-edge of aqueous K^+. The black curve on the left represents the experimental partial electron yield spectrum of K^+ obtained after integrating over the kinetic energies of the Auger electrons in the energy range presented on the figure. The upper panel shows two spectra at photon energies 3610.7 eV, and 3616 eV below and above the ionization potential at 3611.9 eV, respectively. The vertical bars in the resonant Auger spectrum measured at 3610.7 eV indicate the energy positions of the theoretical final $2p^{-2}$ 3d (blue) and $2p^{-2}4p$ (red) resonant Auger states of $K^+(H_2O)_6$ of doublet spin multiplicity. The features A, B and C are discussed in the text.
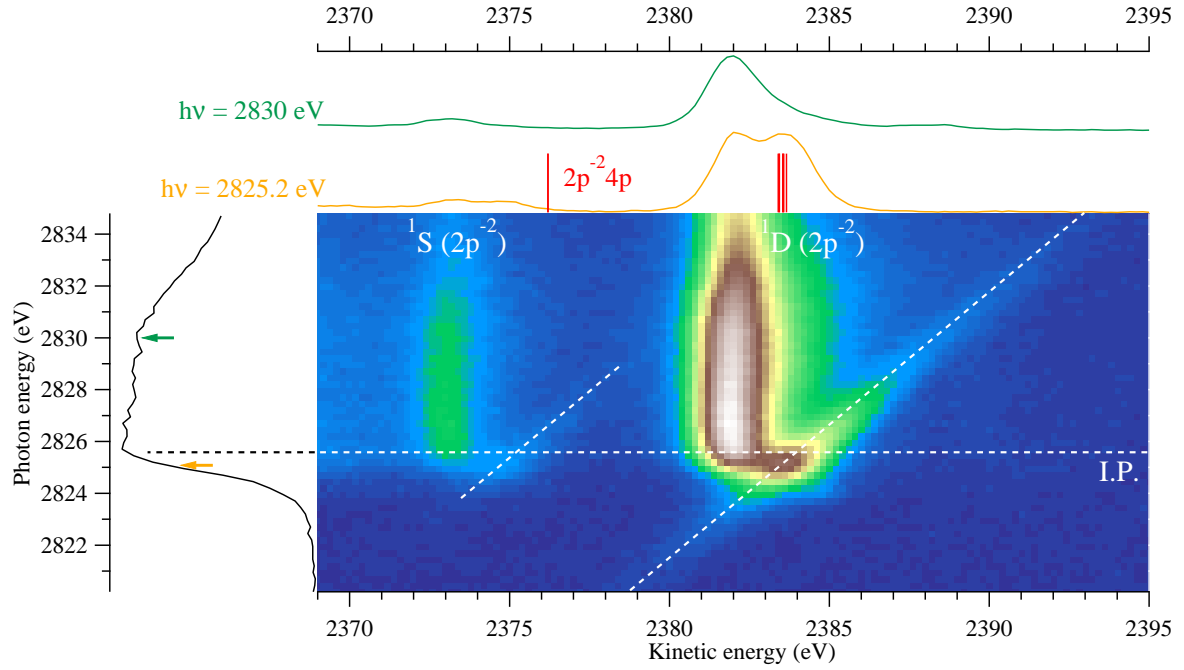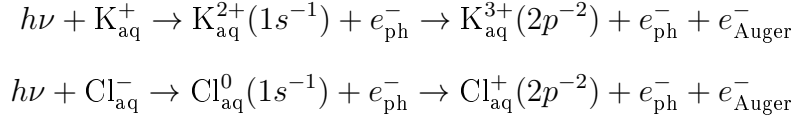
Figure 3: 2D map showing the kinetic energy of the electrons emitted in $KL_{2,3}L_{2,3}$ Auger decay vs the photon energy in the vicinity of the K-edge of aqueous Cl^-. The black curve on the left represents the experimental partial electron yield spectrum of Cl^- obtained after integrating over the kinetic energies of the Auger electrons in the energy range presented on the figure. The upper panel shows two spectra at photon energies 2825.2 eV, and 2830.0 eV below and above the ionization potential at 2825.4 eV, respectively. The vertical bars in the resonant Auger spectrum at 2825.2 eV indicate the energy positions of the theoretical $2p^{-2}4p$ states of $Cl^-(H_2O)_6$ of doublet spin multiplicity.

Normal Auger decay

The $KL_{2,3}L_{2,3}$ normal Auger decay following K-shell ionization of aqueous K^+ and Cl^- can be written as follows

$$h\nu + K^+_{aq} \rightarrow K^{2+}_{aq}(1s^{-1}) + e^-_{ph} \rightarrow K^{3+}_{aq}(2p^{-2}) + e^-_{ph} + e^-_{Auger}$$

$$h\nu + Cl^-_{aq} \rightarrow Cl^0_{aq}(1s^{-1}) + e^-_{ph} \rightarrow Cl^+_{aq}(2p^{-2}) + e^-_{ph} + e^-_{Auger}$$

It populates the $2p^{-2}(^3P, {}^1D, {}^1S)$ final states. The ^3P final states are expected to have a very low intensity since the corresponding transitions are forbidden from angular momentum and parity conservation rules. However, these states are not observed in the experimental spectra presented on Figs. 2 and 3 because they overlap with the $2p^{-2}(^1D)$ and $2p^{-2}(^1D)V'$ states in the kinetic energy region where they are expected to occur. In the case of K^+_{aq} the maxima of the ^1S and ^1D $KL_{2,3}L_{2,3}$ Auger lines are located at 2958 eV and 2968.4 eV, respectively (see Fig. 2). For Cl^-_{aq}, the lines corresponding to the Cl^+ $2p^{-2}(^1S)$ and (^1D) states are located at 2373.2 eV and 2382.1 eV kinetic energy (see Fig. 3). Which photon energy?

The $KL_{2,3}L_{2,3}$ normal Auger lines may disperse with photon energy close to threshold due to energy exchange between the photoelectron and Auger electron called post-collision interaction (PCI). As a result of this interaction, first, an Auger peak becomes asymmetric with a high kinetic energy shoulder, and second, its intensity maximum is shifted to higher kinetic energies close to threshold[50,51]. These effects are seen in our spectra – the asymmetric tail of the peaks resulting from PCI is clearly shown on the resonant Auger spectra at photon energies 3616 eV in the case of K^+, and 2830 eV in the case of Cl^-.

Gunnar: Including this discussion will invite questions about the energy calibration, and IâĂŹm not sure how this was done in these cases. Photoinduced charging may introduce shifts, that can vary with cross section
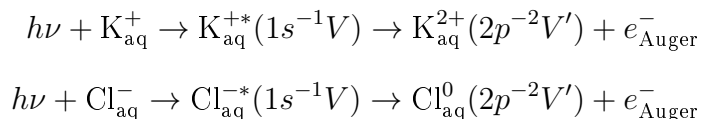
Further, we compare the positions of the normal KLL Auger lines of both Cl^-_{aq} and K^+_{aq} close to threshold with those recorded far from threshold, at photon energies $h\nu = 5$ keV (see

11

Ref.[8] for details). In the latter case, the maxima of the ^{1}D and ^{1}S states appear at 2381.1 eV and 2372.3 eV for Cl^-_{aq}, and 2967.4 eV and 2957 eV for K^+_{aq}, respectively. The maxima were found to be shifted by $\sim$1 eV towards lower kinetic energies as compared to the spectra measured close to threshold. The magnitude of the shift is constant in the photon energy range of XX eV above threshold. Moreover, it is the same for both ions suggesting that it does not depend on the initial charge of the ion. A possible explanation of the shift observed in our experiment is given in Ref.,[52] which focuses on the Auger decay of large Kr clusters close to the $3d_{5/2}$ ionization threshold. The observed $4p^{-2}$(^{1}S, ^{1}D, ^{3}P) Auger peaks were found to be shifted by 0.7 eV to higher kinetic energies compared to the positions of the peaks far above threshold. Moreover, the shift did not vary with the photon energy close to threshold. Consequently, it was proposed that these features originate from a process of internal ionization, i.e. excitation of the photoelectron into the conduction band, followed by normal Auger decay. The observed shift was explained as resulting from the PCI-like interaction between the electron excited in the conduction band and the Auger electron. Further investigations are, however, planned in the case of liquid samples.

Finally, the normal Auger ^{1}D main line of K^+ differs from that of Cl^- by the presence of a large shoulder (feature A on Fig. 2) on the low kinetic energy side at about 2965 eV kinetic energy. This shoulder is attributed to electron transfer from the solvent water molecules to the unoccupied 3d orbitals of K^+ [8]. In the case of Cl^-, there is no experimental evidence of such intense electron transfer processes.

Resonant Auger decay

The $KL_{2,3}L_{2,3}$ Auger decay following resonant K-shell excitation of solvated K^+ and Cl^- can be written as follows

$$h\nu + K^+_{aq} \rightarrow K^{+*}_{aq}(1s^{-1}V) \rightarrow K^{2+}_{aq}(2p^{-2}V') + e^-_{Auger}$$

$$h\nu + Cl^-_{aq} \rightarrow Cl^{-*}_{aq}(1s^{-1}V) \rightarrow Cl^0_{aq}(2p^{-2}V') + e^-_{Auger}$$

where V and V' denote the unoccupied orbitals in the presence of the $1s^{-1}$ and $2p^{-2}$ core holes, respectively. The character of these states is discussed below.

The pre-edge regions of the x-ray absorption spectra of K^+ and Cl^- shown in the left panels of Figs. 2 and 3 do not exhibit any high intensity peaks owing to the lifetime broadening and energetic proximity of the core excited states to the ionization threshold. Consequently, solely from these absorption spectra, one cannot conclude whether there are core excited states in the pre-edge structure. Instead these states have to be identified by their resonant Auger features which differ from the normal Auger features of core ionized states. Thus, for Cl^-, the lowest core excited state is located at 2825.2 eV, which agrees very well with the position of the Cl^- $1s \rightarrow 4p$ excitation determined from Cl K-edge XAS experiments in $MgCl_2.6H_2O$ and of $SrCl_2/SrCl_2.6H_2O$[53] and MCl_4^- compounds[54]. In the case of K^+, there are two dispersive features with maxima at photon energies of 3611.2 eV (B) and 3611.6 eV (C), respectively (Fig. 2). The positions of these two core excited states are close to the energy of the $1s^{-1}4p$ excitation in bare K^+ at 3610.7 eV[55].

The resonant Auger features produced in the decay of these core excited states are quite different for Cl^- and K^+. In the 2D map of Cl^- shown in Fig. 3 there are two dispersive features, indicated with diagonal dashed lines, each on the high kinetic energy side of the ^1S and ^1D main lines. The maxima of these features are at 2825.2 eV photon energy and 2374.6 and 2383.4 eV kinetic energy, respectively. In the case of K^+ (see Fig. 2), the dispersive line related to the ^1S main line cannot be clearly identified due to the presence of strong background. Instead two dispersive features related to the ^1D main line are observed (features B and C indicated with diagonal dashed lines on Fig. 2). Feature B exhibits a maximum at $h\nu =$ 3611.2 eV and 2969.2 eV kinetic energy. The additional feature C appears as a separate island away from the main lines on the 2D map of K^+. It is located at $h\nu =$ 3611.6 eV and 2978.1 eV kinetic energy, thus it is separated by approximately 400 meV in photon energy and 8.3 eV in kinetic energy from the maximum of feature B.

In order to rationalize the pre-edge region of the experimental XAS spectra and the
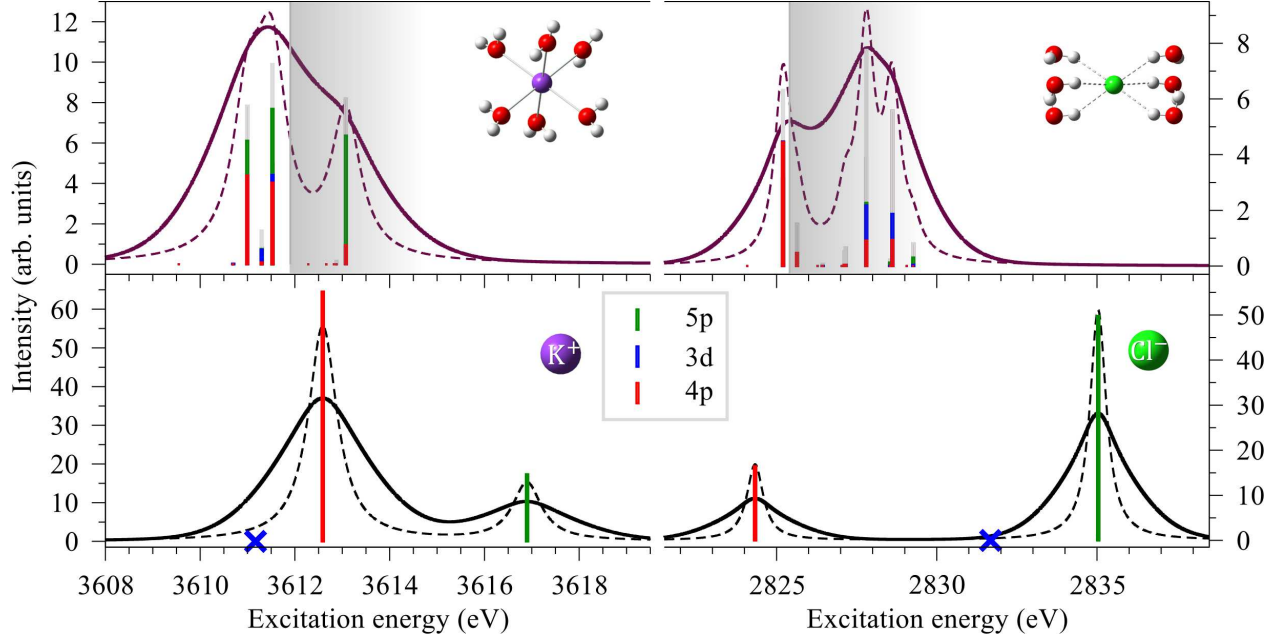
Figure 4: XAS spectra of the lowest K-shell resonant transitions in the bare K^+ (lower left panel) and Cl^- (lower right panel) ions and their 6-coordinated clusters (upper left panel, $K^+(H_2O)_6$, and upper right panel, $Cl^-(H_2O)_6$). The theoretical stick spectra were convolved with a Lorentzian profile of FWHM 0.74 eV for K^+ and 0.62 eV for Cl^- (dashed line)[8] and a Voigt profile to account for the lifetime broadening and the experimental resolution (full line). The stick spectrum corresponds to the projections $|a_{nl}^i|^2$ of the SONOs corresponding to the core excited states of the 6-coordinated clusters on the basis of SONOs corresponding to the $1s^{-1}3d$, $1s^{-1}4p$, and $1s^{-1}5p$ states in the bare K^+ and Cl^- ions (Eq. 1). The grey sticks in the stick spectrum correspond to contributions from higher-lying atomic core excitations or from excitations to the solvent molecules. The theoretical XAS spectra of both K^+ and Cl^- were shifted to higher photon energies such that the excitation energies of the lowest core excited states correspond to the experimentally determined energies – 3610.7 eV in the case of K^+, and 2825.2 eV in the case of Cl^-. The experimental ionization thresholds are depicted as grey boxes starting at photon energies of 3611.9 eV (K^+_{aq}) and 2825.4 eV (Cl^-_{aq}).

differences in the AES spectra of K^+_{aq} and Cl^-_{aq}, we computed the lowest core excited states of the bare K^+ and Cl^- ions and their hexa-coordinated clusters. The theoretical XAS spectra are presented in Fig. 4. In the bare ions (lowermost panels on Fig. 4), the lowest energy peak corresponds to the dipole allowed $1s^{-1}4p$ state. The next dipole allowed state, $1s^{-1}5p$, is located 4.3 eV and 10.8 eV higher in the cases of K^+ and Cl^-, respectively. Together with the two dipole allowed transitions, we show the dipole forbidden $1s^{-1}3d$ states of the bare ions as blue crosses at photon energies 3611.17 eV in the case of K^+ and 2831.68 eV

14

in the case of Cl$^-$, respectively. It is noteworthy that the positions of the 1s^{-1}4p and 1s^{-1}3d states are inverted in K$^+$ and Cl$^-$. In the case of Cl$^-$ the 1s^{-1}4p excitation has lower energy and the 1s^{-1}3d excitation is close to the 1s^{-1}5p state. On the contrary, in K$^+$ the 1s^{-1}3d excitation has lower energy and lies below the 1s^{-1}4p state. We note in passing that the intensity of the Cl$^-$(1s^{-1}4p) state is lower than that of the Cl$^-$(1s^{-1}5p) state contrary to what is observed in K$^+$. This difference can be explained by the lower electron density of the 4p compared to the 5p electron in the region close to the core hole which thus results in the lower oscillator strength of the 1s^{-1}4p compared to the 1s^{-1}5p transition in Cl$^-$ (see Fig. 1 in SI).

The water molecules in the first solvation shell have several effects on the core excited states. First, upon addition of water molecules, the degeneracy of the 1s^{-1}4p state is lifted and the intensity of the resulting states in the cluster drops. Moreover, the character of these states changes as can be seen on the upper panels of Fig. 4. They are no longer of pure atomic character but they rather interact with states of the neighboring water molecules (shown as grey bars in Fig. 4) and with other closely lying states of the bare ion, such as the dipole allowed 1s^{-1}5p and dipole forbidden 1s^{-1}3d state. Thus, the latter also acquire intensity in the cluster due to mixing with the dipole allowed states in the ligand field of the solvent. A similar effect was observed in the XAS spectra of microsolvated clusters of Na$^+$ and Mg^{2+} [18].

Further we assume that only the lowest peak in the theoretical XAS spectra is populated in the experiment for two reasons. First, due to the lifetime broadening, it spreads over approximately 2 eV which coincides with the width of the pre-edge structure in the experimental XAS spectra. Second, the splitting between the first core excited state and the ionization threshold in the experiment is 1.2 eV for K$^+$ and 0.2 eV for Cl$^-$, and thus it is smaller than the splitting between the first and second peak in the theoretical spectra (1.5 eV for K$^+$ and ~3 eV for Cl$^-$, Fig. 4). In the 6-coordinated cluster (Fig. 4 upper left panel), which represents the complete first solvation shell around K$^+$, the lowest peak in the spec-

trum contains three states. The lowest and highest lying states are split by approximately 0.5 eV and they have mixed 4p and 5p character. The low intensity state in between these two states has a predominantly $1s^{-1}3d$ character. Since the dispersive feature B appears at lower excitation energies compared to the feature C, we assume that it is produced in the resonant Auger decay of the lowest core excited states of K^+, which are predominantly of $1s^{-1}4p$ character. Moreover, we can attribute the feature C to the resonant Auger decay of the low intensity dipole forbidden $1s^{-1}3d$ state. Thus, we explain both the energy splitting of ~400 meV photon energy of the two features, and the fact that island C has lower intensity than feature B (Fig. 2).

In the hexa-coordinated cluster of Cl^-, the solvent molecules have little influence on the position and character of the first state. Due to the large energy separation from other Cl^- states it has mainly Cl^- $1s^{-1}4p$ character with some admixture of states of the nearest water molecules. We therefore attribute the two dispersive features associated with the ^1S and ^1D main lines on the 2D map of Cl^- to the resonant Auger decay of this core excited state involving mostly the 4p orbitals of chloride.

To fully characterize the dispersive features on the experimental 2D maps, we also computed the lowest $K^{2+}[2p^{-2}nl](H_2O)_6$ and $Cl^0[2p^{-2}nl](H_2O)_6$ states of the hexa-coordinated clusters corresponding to the lowest final spectator resonant Auger states. The energy positions of these lines are shown as bars on the experimental resonant Auger spectra in the upper panels of Figs. 2 and 3. In both cases, we shifted the lowest $2p^{-2}(^1D)4p$ states such that the kinetic energies coincide with the maxima of the dispersive features on the high kinetic energy part of the ^1D main line. Note that we only indicate resonant Auger transitions to the spin-allowed final states of doublet multiplicity. Since the initial core excited states are populated by photon excitation, only doublet states are efficiently populated in the resonant Auger decay. The energetic positions of the $2p^{-2}nl$ states of $K^+(H_2O)_6$ and $Cl^-(H_2O)_6$ are substantially different, reflecting the fact that the 3d unoccupied orbitals of K^+ are lower than the 4p orbitals. This is the opposite of what is observed in Cl^-, where

the $2p^{-2}3d$ states (not shown) are located on the lower kinetic energy side of the respective $2p^{-2}4p$ states.

As mentioned above, we attribute the island B to the decay of the lowest lying core excited state, which has predominantly $1s^{-1}4p$ character. Supposing that this state undergoes mostly pure spectator resonant Auger decay, which is the case of the $1s^{-1}4p$ state in the isoelectronic Ar atom[56], then the lowest states of $2p^{-2}4p$ character are populated resulting in resonant Auger lines located between 2969 and 2970.5 eV. As can be seen from the Auger electron spectrum at $h\nu = 3610.7$ eV (upper panel of Fig. 2), the lowest $2p^{-2}4p$ states of $K^+(H_2O)_6$ starting at electron energy of 2969 eV are separated by $\sim$5 and 12-13 eV from the two groups of $2p^{-2}3d$ states located at higher electron kinetic energies. Thus, the group of $2p^{-2}3d$ states at $\sim$2975 eV lies closer to the position of island C. Consequently, we attribute this dispersive feature as originating from the resonant Auger decay of the $1s^{-1}3d$ excitation to the group of $2p^{-2}3d$ states lying around 2975 eV. The splitting between the $2p^{-2}4p$ and $2p^{-2}3d$ states in our calculation is smaller than the splitting between the islands B and C. This difference may be due to the fact that we do not account for the effect of distant solvent shells in our calculation. Concerning the higher lying group of $2p^{-2}3d$ states at kinetic energies between 2982 and 2983 eV, we conclude that these states are not populated via the Auger process since no additional experimental features are observed.

The energy difference between the spectral features A and C provides another argument in favor of the $2p^{-2}\,3d$ character of the feature C. The feature A originates from electron transfer processes from water molecules (W) to the doubly core ionized potassium ion and has the configuration $K^{2+}(2p^{-2}3d)W^{-1}$. The lowest ionization potential of liquid water in the liquid phase is about 11.16 eV[57] which fits well with the observed A-C splitting. Based on the above energetic arguments we attribute the island C as originating from resonant Auger decay to the $K^{2+}\,2p^{-2}3d$ final state.

In the computed $Cl^0[2p^{-2}nl](H_2O)_6$ spectrum there are two groups of states split by about 7 eV (see upper panel of Fig. 3). The lower kinetic energy group corresponds to

the $2p^{-2}(^1S)4p$ final states, whereas the higher kinetic energy group corresponds to the $2p^{-2}(^1D)4p$ final states. The splitting between these two groups is in good agreement with the experimental splitting between the dispersive features on the high kinetic energy sides of the ^1S and ^1D main peaks. Consequently, we attribute these dispersive features as resulting from the resonant Auger decay of the $1s^{-1}4p$ core excited state of Cl^-_{aq} to the $2p^{-2}(^1S)4p$ and $2p^{-2}(^1D)4p$ final states. Similar dispersive features originating from the decay of the Cl $(1s^{-1}4p)$ state were observed on the 2D map of chloromethane CH_3Cl recorded in the vicinity of the Cl K-edge in gas phase.[58] In this case, however, additional lower-lying core excited states are observed. They result from excitation to the LUMO of CH_3Cl, which is a linear combination of the C 2p and Cl 3p atomic orbitals. Since the 3p shell is fully occupied in Cl^-, such core excited states are not observed in our experiment. We note that neither $2p^{-2}3d$ nor charge transfer states are found in the Cl^-_{aq} case.

Delocalization vs resonant Auger decay

As mentioned above, the delocalization of core excited electrons in aqueous solutions is ultrafast and as such it competes with the resonant Auger decay. In order to estimate the delocalization rate of the core excited electron at the pre-edges of K^+ and Cl^-, we used the core-hole clock method.[59,60]

In the case of Cl^-, it was possible to perform the same data treatment as in Ref.[56] i.e., for each photon energy step, all components of the 2D map shown in Fig. 3 were isolated by fitting procedures and their intensity integrated to get a partial electron yield as a function of the photon energy. The result is shown on Fig. 2 in the SI. The figure shows that there is a large overlap between the resonant and normal Auger contributions, due to the proximity of the resonance to the ionization potential and due to the very short lifetime of the corresponding states. At the specific photon energy corresponding to the lowest core excitation, $h\nu = 2825.2\,\mathrm{eV}$ (Fig. 3, upper panel) a double-peak structure is observed in the interval of kinetic energies $2380 - 2385\,\mathrm{eV}$. The position of the first peak coincides with

18

the ^{1}D main line resulting from normal Auger decay, whereas the second peak at $2383.5\,\mathrm{eV}$ corresponds to the resonant Auger decay to the $2\mathrm{p}^{-2}(^1\mathrm{D})4\mathrm{p}$ states. By fitting this double-peak structure with two Voigt functions, we determine the ratio of the intensities of these peaks to be $l/d \approx 1$. From the ratio l/d and the Auger lifetime τ_c, one can determine the delocalization time τ_CT according to the relation $\tau_\mathrm{CT} = \tau_c l/d$ [61]MORE REFS. Consequently, the delocalization time τ_CT is of the same order as the Auger lifetime, i.e. $\sim 1\,\mathrm{fs}$. The fast delocalization in this case is a result of the fact that the energy splitting between the Cl^- ($1\mathrm{s}^{-1}4\mathrm{p}$) resonance and the ionization threshold is $0.2\,\mathrm{eV}$, and thus, smaller than the lifetime broadening of $0.62\,\mathrm{eV}$ [8].

For potassium, the treatment is more complex due to the presence of multiple simultaneous processes – normal, resonant Auger decay, charge transfer from solvent. To extract the intensity of each component from the 2D map shown in Fig. 2, one needs the spectral fingerprints of each process to be separated. However, as can be seen, this is hardly possible especially close to threshold in the kinetic energy region $2965 - 2970\,\mathrm{eV}$. For instance at $3610.7\,\mathrm{eV}$ photon energy on the high-kinetic-energy side of the ^{1}D main line, there are contributions from the PCI tail and from the $2\mathrm{p}^{-2}(^1\mathrm{D})4\mathrm{p}$ resonant Auger state. On the low-kinetic-energy side, the charge transfer processes lead to a very large structure whose shape unfortunately cannot be easily simulated by a known profile. However, the lifetime of the 1s core hole is shorter for potassium than for chloride (0.9 vs. $1\,\mathrm{fs}$) and, moreover, the core excited state appears $1.2\,\mathrm{eV}$ below the ionization threshold whereas it is only $0.2\,\mathrm{eV}$ for chloride. Therefore, one can expect much less efficient delocalization compared to $\mathrm{Cl}^-_\mathrm{aq}$.

Conclusion

Using a combination of x-ray absorption and Auger electron spectroscopy in the tender x-ray regime, we studied the electronic structure of aqueous solution of KCl at the K-edges of both K and Cl. The Auger electron spectra of both ions as a function of photon energy exhibit

features of normal as well as resonant Auger processes. To interpret the resonant Auger features in the experimental spectrum, we performed *ab initio* calculations on microsolvated clusters of K^+ and Cl^-. Our calculations show that the energy ordering of the 3d and 4p virtual orbitals of Cl^- is inverted compared to K^+, and also that the energy splitting between the bright $1s^{-1}4p$ and dark $1s^{-1}3d$ core excited states is larger in the chloride case. Thus, the energetic proximity of the 3d and 4p orbitals in the bare K^+ ion results in the dipole forbidden $1s^{-1}3d$ state acquiring intensity in a solution as a result of mixing with the dipole allowed $1s^{-1}4p$ excitation. The spectator Auger decay of this state produces an additional dispersive feature which is manifested as a separate peak in the Auger electron spectrum at high kinetic energies. In the case of Cl^- the $1s^{-1}4p$ and $1s^{-1}3d$ core excited states do not interact, and therefore, only fingerprints of the population and Auger decay of the dipole allowed $1s^{-1}4p$ excitation are observed in the spectrum. Moreover, using the core-hole clock method we estimated the time of delocalization of the core excited electron at the pre-edge region of Cl^-_{aq}. Our results show that in this case, the resonant Auger decay and the delocalization of the excited electron occur on a comparable timescale. In the case of K^+_{aq}, we cannot make an accurate estimate, however, one can expect a much less efficient delocalization of the core excited electron.

Our work shows that the combination of x-ray absorption and resonant Auger spectroscopy is a sensitive probe of the electronic structure of solvated ions. The reported results are an important first step in the study of the chains of relaxation steps triggered by photoabsorption in the tender x-ray regime. The Auger processes considered in this work are inevitably followed by multiple intra- and interatomic electronic decays, such as interatomic Coulombic decay (ICD) and electron-transfer mediated decay (ETMD). As a result of the latter processes, genotoxic free radicals and slow electrons are formed in the vicinity of the metal center. The magnitude of the damage inflicted upon the environment and the energies of the emitted electrons depend on the initial Auger step, and can therefore be controlled by tuning the energy of the radiation. Consequently, the results of this work can have impli-

cations in understanding radiation chemistry and radiation damage in biologically relevant systems.

Acknowledgement

Supporting Information Available

- suppinfo.pdf: contains 1) the radial density distributions of the core excited states of the bare ions; 2) partial cross sections and charge transfer time extracted from the experimental 2D map near the Cl 1s edge.

References

(1) Smith, J. W.; Saykally, R. J. *Chem. Rev.* **2017**, *117*, 13909–13934, PMID: 29125751.

(2) O'Neill, P.; Stevens, D. L.; Garman, E. F. *J. Synchrotron Radiat.* **2002**, *9*, 329–332.

(3) Carugo, O.; Carugo, K. D. *Trends Biochem. Sci.* **2005**, *30*, 213–219.

(4) Stumpf, V.; Gokhberg, K.; Cederbaum, L. S. *Nat. Chem.* **2016**, *8*, 237–241.

(5) Pokapanich, W.; Bergersen, H.; Bradeanu, I. L.; Marinho, R. R. T.; Lindblad, A.; Legendre, S.; Rosso, A.; Svensson, S.; Björneholm, O.; Tchaplyguine, M.; Öhrwall, G.; Kryzhevoi, N. V.; Cederbaum, L. S. *J. Am. Chem. Soc.* **2009**, *131*, 7264–7271.

(6) Pokapanich, W.; Kryzhevoi, N. V.; Ottosson, N.; Svensson, S.; Cederbaum, L. S.; Öhrwall, G.; Björneholm, O. *J. Am. Chem. Soc.* **2011**, *133*, 13430.

(7) Unger, I.; Seidel, R.; Thürmer, S.; Pohl, M. N.; Aziz, E. F.; Cederbaum, L. S.; Muchová, E.; Slavíček, P.; Winter, B.; Kryzhevoi, N. V. *Nat. Chem.* **2017**, *9*, 708.

(8) Céolin, D.; Kryzhevoi, N. V.; Nicolas, C.; Pokapanich, W.; Choksakulporn, S.; Songsiriritthigul, P.; Saisopa, T.; Rattanachai, Y.; Utsumi, Y.; Palaudoux, J.; Öhrwall, G.; Rueff, J.-P. *Phys. Rev. Lett.* **2017**, *119*, 263003.

(9) Stoychev, S. D.; Kuleff, A. I.; Tarantelli, F.; Cederbaum, L. S. *J. Chem. Phys.* **2008**, *129*, 074307.

(10) Demekhin, P. V.; Scheit, S.; Stoychev, S. D.; Cederbaum, L. S. *Phys. Rev. A* **2008**, *78*, 043421.

(11) Demekhin, P. V.; Chiang, Y.-C.; Stoychev, S. D.; Kolorenč, P.; Scheit, S.; Kuleff, A. I.; Tarantelli, F.; Cederbaum, L. S. *J. Chem. Phys.* **2009**, *131*, 104303.

(12) Ouchi, T.; Sakai, K.; Fukuzawa, H.; Higuchi, I.; Demekhin, P. V.; Chiang, Y.-C.; Stoychev, S. D.; Kuleff, A. I.; Mazza, T.; Schöffler, M.; Nagaya, K.; Yao, M.; Tamenori, Y.; Saito, N.; Ueda, K. *Phys. Rev. A* **2011**, *83*, 053415.

(13) Miteva, T.; Chiang, Y.-C.; Kolorenč, P.; Kuleff, A. I.; Cederbaum, L. S.; Gokhberg, K. *J. Chem. Phys.* **2014**, *141*, 164303.

(14) Travnikova, O.; Marchenko, T.; Goldsztejn, G.; Jänkälä, K.; Sisourat, N.; Carniato, S.; Guillemin, R.; Journel, L.; Céolin, D.; Püttner, R.; Iwayama, H.; Shigemasa, E.; Piancastelli, M. N.; Simon, M. *Phys. Rev. Lett.* **2016**, *116*, 213001.

(15) Gokhberg, K.; Kolorenč, P.; Kuleff, A. I.; Cederbaum, L. S. *Nature* **2014**, *505*, 661–663.

(16) Trinter, F. et al. *Nature* **2014**, *505*, 664–666.

(17) Björneholm, O.; Federmann, F.; Fössing, F.; Möller, T. *Phys. Rev. Lett.* **1995**, *74*, 3017–3020.

(18) Miteva, T.; Wenzel, J.; Klaiman, S.; Dreuw, A.; Gokhberg, K. *Phys. Chem. Chem. Phys.* **2016**, *18*, 16671–16681.

(19) Nordlund, D.; Ogasawara, H.; Bluhm, H.; Takahashi, O.; Odelius, M.; Nagasono, M.; Pettersson, L. G. M.; Nilsson, A. *Phys. Rev. Lett.* **2007**, *99*, 217406.

(20) Ottosson, N.; Odelius, M.; Spångberg, D.; Pokapanich, W.; Svanqvist, M.; Öhrwall, G.; Winter, B.; Björneholm, O. *J. Am. Chem. Soc.* **2011**, *133*, 13489–13495.

(21) Wagner, C. D.; Zatko, D. A.; Raymond, R. H. *Anal. Chem.* **1980**, *52*, 1445–1451.

(22) Céolin, D.; Ablett, J.; Prieur, D.; Moreno, T.; Rueff, J.-P.; Marchenko, T.; Journel, L.; Guillemin, R.; Pilette, B.; Marin, T.; Simon, M. *J. Electron Spectrosc. Relat. Phenom.* **2013**, *190, Part B*, 188 − 192.

(23) Rueff, J.-P.; Ablett, J. M.; Céolin, D.; Prieur, D.; Moreno, T.; Balédent, V.; Lassalle-Kaiser, B.; Rault, J. E.; Simon, M.; Shukla, A. *J. Synchrotron Rad.* **2015**, *22*, 175–179.

(24) Faubel, M.; Schlemmer, S.; Toennies, J. P. *Z. Phys. D* **1988**, *10*, 269–277.

(25) Winter, B.; Faubel, M. *Chem. Rev.* **2006**, *106*, 1176–1211, PMID: 16608177.

(26) Ohtaki, H.; Radnai, T. *Chem. Rev.* **1993**, *93*, 1157–1204.

(27) Soper, A. K.; Weckström, K. *Biophys. Chem.* **2006**, *124*, 180 − 191.

(28) Ma, H. *Int. J. Quant. Chem.* **2014**, *114*, 1006–1011.

(29) Krishnan, R.; Binkley, J. S.; Seeger, R.; Pople, J. A. *J. Chem. Phys.* **1980**, *72*, 650–654.

(30) Blaudeau, J.-P.; McGrath, M. P.; Curtiss, L. A.; Radom, L. *J. Chem. Phys.* **1997**, *107*, 5016–5021.

(31) Frisch, M. J. et al. Gaussian 09 Revision D.01. Gaussian Inc. Wallingford CT 2009.

(32) Lee, H. M.; Kim, J.; Lee, S.; Mhin, B. J.; Kim, K. S. *J. Chem. Phys.* **1999**, *111*, 3995–4004.

(33) Lee, H. M.; Kim, D.; Kim, K. S. *J. Chem. Phys.* **2002**, *116*, 5509–5520.

(34) Ge, L.; Bernasconi, L.; Hunt, P. *Phys. Chem. Chem. Phys.* **2013**, *15*, 13169–13183.

(35) Gora, R. W.; Roszak, S.; Leszczynski, J. *Chem. Phys. Lett.* **2000**, *325*, 7 – 14.

(36) Schirmer, J. *Phys. Rev. A* **1982**, *26*, 2395–2416.

(37) Barth, A.; Schirmer, J. *J. Phys. B At. Mol. Opt. Phys.* **1985**, *18*, 867.

(38) Cederbaum, L. S.; Domcke, W.; Schirmer, J. *Phys. Rev. A* **1980**, *22*, 206–222.

(39) Barth, A.; Cederbaum, L. S. *Phys. Rev. A* **1981**, *23*, 1038–1061.

(40) Wenzel, J.; Wormit, M.; Dreuw, A. *J. Comp. Chem.* **2014**, *35*, 1900–1915.

(41) Wenzel, J.; Wormit, M.; Dreuw, A. *J. Chem. Theory Comput.* **2014**, *10*, 4583–4598.

(42) Wormit, M.; Rehn, D. R.; Harbach, P. H.; Wenzel, J.; Krauter, C. M.; Epifanovsky, E.; Dreuw, A. *Mol. Phys.* **2014**, *112*, 774–784.

(43) Shao, Y. et al. *Mol. Phys.* **2015**, *113*, 184–215.

(44) McLean, A. D.; Chandler, G. S. *J. Chem. Phys.* **1980**, *72*, 5639–5648.

(45) Krause, M. O.; Oliver, J. H. *J. Phys. Chem. Ref. Data* **1979**, *8*, 329–338.

(46) Brooks, B. R.; Laidig, W. D.; Saxe, P.; Handy, N. C.; Schaefer III, H. F. *Phys. Scr.* **1980**, *21*, 312.

(47) Brooks, B. R.; Schaefer, H. F. *J. Chem. Phys.* **1979**, *70*, 5092–5106.

(48) Schmidt, M. W.; Baldridge, K. K.; Boatz, J. A.; Elbert, S. T.; Gordon, M. S.; Jensen, J. H.; Koseki, S.; Matsunaga, N.; Nguyen, K. A.; Su, S.; Windus, T. L.; Dupuis, M.; Montgomery, J. A. *J. Comp. Chem.* **1993**, *14*, 1347–1363.

(49) Mosnier, J.-P.; Kennedy, E. T.; van Kampen, P.; Cubaynes, D.; Guilbaud, S.; Sisourat, N.; Puglisi, A.; Carniato, S.; Bizau, J.-M. *Phys. Rev. A* **2016**, *93*, 061401.

(50) Russek, A.; Mehlhorn, W. *J. Phys. B At. Mol. Opt. Phys.* **1986**, *19*, 911.

(51) Guillemin, R.; Sheinerman, S.; Püttner, R.; Marchenko, T.; Goldsztejn, G.; Journel, L.; Kushawaha, R. K.; Céolin, D.; Piancastelli, M. N.; Simon, M. *Phys. Rev. A* **2015**, *92*, 012503.

(52) Tchaplyguine, M.; Kivimäki, A.; Peredkov, S.; Sorensen, S. L.; Öhrwall, G.; Schulz, J.; Lundwall, M.; Rander, T.; Lindblad, A.; Rosso, A.; Svensson, S.; Mårtensson, N.; Björneholm, O. *J. Chem. Phys.* **2007**, *127*, 124314.

(53) Sugiura, C. *J. Chem. Phys.* **1982**, *77*, 681–682.

(54) Shadle, S. E.; Hedman, B.; Hodgson, K. O.; Solomon, E. I. *J. Am. Chem. Soc.* **1995**, *117*, 2259–2272.

(55) Hertlein, M. P.; Adaniya, H.; Amini, J.; Bressler, C.; Feinberg, B.; Kaiser, M.; Neumann, N.; Prior, M. H.; Belkacem, A. *Phys. Rev. A* **2006**, *73*, 062715.

(56) Céolin, D.; Marchenko, T.; Guillemin, R.; Journel, L.; Kushawaha, R. K.; Carniato, S.; Huttula, S.-M.; Rueff, J. P.; Armen, G. B.; Piancastelli, M. N.; Simon, M. *Phys. Rev. A* **2015**, *91*, 022502.

(57) Winter, B.; Weber, R.; Widdra, W.; Dittmar, M.; Faubel, M.; Hertel, I. V. *J. Phys. Chem. A* **2004**, *108*, 2625–2632.

(58) Goldsztejn, G.; Marchenko, T.; Püttner, R.; Journel, L.; Guillemin, R.; Carniato, S.; Selles, P.; Travnikova, O.; Céolin, D.; Lago, A. F.; Feifel, R.; Lablanquie, P.; Piancastelli, M. N.; Penent, F.; Simon, M. *Phys. Rev. Lett.* **2016**, *117*, 133001.

(59) Björneholm, O.; Nilsson, A.; Sandell, A.; Hernnäs, B.; Mrtensson, N. *Phys. Rev. Lett.* **1992**, *68*, 1892–1895.

(60) Karis, O.; Nilsson, A.; Weinelt, M.; Wiell, T.; Puglia, C.; Wassdahl, N.; Mårtensson, N.; Samant, M.; Stöhr, J. *Phys. Rev. Lett.* **1996**, *76*, 1380–1383.

(61) Föhlisch, A.; Feulner, P.; Hennies, F.; Fink, A.; Menzel, D.; Sanchez-Portal, D.; Echenique, P. M.; Wurth, W. *Nature* **2005**, *436*, 373.

Graphical TOC Entry